Exp Fluids (2011) 50:1625–1632
DOI 10.1007/s00348-010-1019-5

RESEARCH ARTICLE

Scalar interactions between parallel jets measured using a two-channel PLIF technique

M. A. Soltys · J. P. Crimaldi

Received: 7 April 2010 / Revised: 27 November 2010 / Accepted: 4 December 2010 / Published online: 17 December 2010

Abstract A two-channel PLIF technique that simultaneously quantifies two scalar fields is presented. The technique consists of two independently operated single-color PLIF systems that synchronously image a common region. Two dyes (fluorescein sodium salt and oxazine 725) are excited by two lasers (argon-ion and krypton-ion), and the resulting fluorescence is imaged by a pair of cameras. The two-channel system is used to study mixing between two parallel jets, each transporting a different scalar species. Time-averaged and instantaneous mixing statistics are calculated and used to show the effects of turbulent structure on scalar mixing. In particular, the existence of positive spatial correlations between the two scalar fields is demonstrated in off-axis mixing regions.

1 Introduction

Interactions between multiple jets are of interest for mixing studies in the areas of combustion, chemical mixing, pollutant transport, and environmental processes. Velocity fields for multiple jets have been studied for parallel jets (Yuu et al. 1979; Pani and Dash 1983; Fujisawa et al. 2004), inclined jets (Becker and Booth 1975; Wang et al. 1993), and coaxial jets (Champagne and Wygnanski 1971). Scalar fields have been measured in multiple plane jets (Grandmaison and Zettler 1989) and multiple round jets (Hodgson et al. 1999; Wang and Davidson 2003). The mixing of multiple scalars emitted from jets has received much less attention. Stapountzis et al. (1992) studied the reaction product of two scalars emitted from parallel jets, but did not quantify the reactant concentration fields themselves. Fujisawa et al. (2004) and Duplat and Villermaux (2008) qualitatively visualized mixing between two parallel jets. We are not aware of any quantitative studies of the interaction between multiple jets that each carry different scalars.

In this study, we introduce a two-channel planar laser-induced fluorescence (PLIF) system capable of simultaneously and independently quantifying two inhomogeneous scalar fields that potentially overlap in space and time. We then use the system to investigate scalar mixing between two parallel jets, where each jet carries a different scalar. Of particular interest from the perspective of mixing and reaction studies is the extent to which the two resulting scalar fields interact and develop spatial correlations due to the presence of coherence in the velocity field.

Planar laser-induced fluorescence is a common technique for visualizing and quantifying scalar transport and mixing in fluid flows. PLIF uses a laser sheet to excite a fluorophore (typically a fluorescent dye) carried in the fluid. The fluoresced light is measured with an imaging device, and fluorescence intensity can then be related to the local concentration of the fluorophore. Most existing implementations use a single dye, where the dye itself is a surrogate for the scalar of interest. Variations have used two dyes, in uniform concentrations throughout the domain, with differing sensitivities to an existing extrinsic scalar, such as pH or temperature, to quantify the scalar (Coppeta and Rogers 1998; Sakakibara and Adrian 1999; Bruchhausen et al. 2005; Robinson et al. 2008). Because these two-dye systems use both dyes to provide information for a single extrinsic scalar in the flow, we refer to such systems herein as "single-channel" PLIF. Existing single-channel PLIF implementations have been used to

M. A. Soltys · J. P. Crimaldi (✉)
Department of Civil and Environmental Engineering,
University of Colorado, Boulder, CO 80309-0428, USA
e-mail: Crimaldi@Colorado.edu

measure mean and fluctuating concentrations of a single scalar in a wide range of applications (see review on aqueous PLIF by Crimaldi 2008).

Existing single-channel PLIF techniques can be used to study mixing between two scalars in the special case where the two scalars fill the entire domain and share a common interface. In this case, the fluorescent dye is a proxy for scalar A and is measured in the same manner as other single-scalar problems. If the two scalar concentrations are non-dimensionalized as mass fractions C_A and C_B, then $C_A + C_B = 1$ everywhere and instantaneous measurements of C_B can be directly inferred from instantaneous measurements of C_A (Cetegen and Sirignano 1990; Crimaldi et al. 2008). For reactive mixing studies, the pH dependence of a fluorescent dye has been exploited to view the mixing or reaction zone (Koochesfahani and Dimotakis 1986; Karasso and Mungal 1997; Cetegen and Mohamad, 1993). In these studies, the single scalar of interest becomes the mixing ratio or the reaction product.

For mixing problems where two scalars are separated by a third fluid (e.g., the two-jet problem investigated in the present study), the ability to independently quantify each of the two scalars is necessary because the measurements of one scalar cannot be used to infer the concentration of the second. Thus, for PLIF, a "two-channel" implementation is required, but few examples exist in the literature. Su and Clemens (1999) introduced a variation on traditional PLIF, which uses PLIF in conjunction with Rayleigh scattering to measure two well-mixed scalars independently in two planes to obtain three-dimensional diffusion rates. This two-channel technique, while able to measure two conserved scalars, is limited to gaseous flows and therefore low Schmidt number problems. Kling and Mewes (2004) developed a technique that uses two fluorophores, one reactive and one inert, along with a single excitation laser to trace micro- and macro-mixing processes in chemical reactors; however, due to the high cost of the fluorophores, this technique is best suited to small-scale applications. In a related two-channel technique, Lavertu et al. (2008) used one excitation laser and highly sensitive photomultiplier tubes to measure differential diffusion between two scalars at a single point. Lehwald et al. (2010) modified the technique of Kling and Mewes (2004) to use less expensive fluorophores. This technique is, in principal, capable of measuring two conserved scalars using a single laser if pH is held constant; however, for higher signal-to-noise, additional excitation power and further spectral separation may be required. The two-channel PLIF technique described in the present study builds on standard single-channel PLIF methodologies to produce a system that simultaneously quantifies two fluorescent dye fields with less than 1% error.

2 Two-channel system

The two-channel PLIF system consists of two independent single-color PLIF systems designed to be run simultaneously in the same space with negligible crosstalk. Two dyes were paired with separate excitation lasers in different regions of the visible light spectrum. The laser beams were combined into a single light sheet that scans the imaging area. A pair of CCD cameras with optical filters matched to each dye's emission spectra recorded instantaneous fluorescence from the two dyes. Images from each camera were then post-processed to yield scalar image pairs corresponding in time and space.

2.1 Optical setup

A schematic of the laser and imaging optics is shown in Fig. 1. Ion lasers are chosen for their stable continuous output and superior beam quality. Choosing the 488 nm argon-ion laser line and the 647.1 nm krypton-ion laser line offers a balance of high power output and a large separation between the two excitation wavelengths. Each laser is operated in a closed-loop light-regulated TEM00 mode. The beams of each laser are kept separate through the initial stages of the optics to minimize chromatic aberration. The beams exit the lasers with Gaussian cross sections 1.5 mm in diameter. Using a zoom beam expander, the beams are expanded 10× and refocused in the imaging area to a width of approximately 0.5 mm at the center of the imaging region and 0.9 mm at the edge of the imaging region. The beams are combined with a dichroic mirror that allows the argon-ion beam to be transmitted while reflecting the krypton-ion beam. The combined beam is then spread into a planer light sheet using a scanning mirror that is synchronized to scan once across the image area for every integration period of the cameras. Tests showed that the laser sheet was sufficiently thin to produce converged scalar statistics for the two-jet experiment in Sect. 3.

Fluorescence is measured using two monochrome 12-bit 1,024 × 1,024 pixel CCD cameras (Dalstar 1M30) with 50 mm lenses. Each camera is fitted with an optical filter corresponding to the emission spectra of the channel it measures, as detailed in Sect. 2.2. One camera is positioned

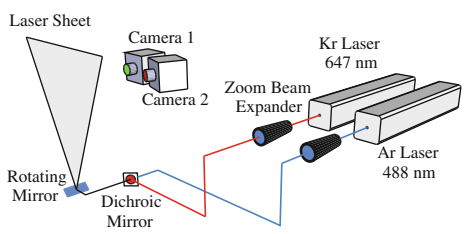

Fig. 1 Laser and imaging optical setup

perpendicular to the light sheet, while the other camera is skewed 5° from perpendicular. Images are rectified to the plane of the light sheet as discussed in Sect. 2.3.

2.2 Dye selection

Primary criteria for dye selection include water solubility, compatibility with available laser excitation, emission wavelengths within the visible spectrum, high quantum efficiency, and adequate Stokes shift (Arcoumanis et al. 1990). Other considerations include sensitivity to temperature and pH, susceptibility to photobleaching, fluorescence linearity with concentration, and toxicity (Crimaldi 2008). For a two dye system, the dyes must be non-reactive and possess absorption/emission spectra that are sufficiently distant to avoid crosstalk. Coppeta and Rogers (1998) identify three types of crosstalk errors that are possible in two-dye systems. Type I errors occur when fluoresced light from PLIF system 1 is directly detected by system 2. Type I errors can be minimized by careful selection of filters and applying a correction algorithm in the post-processing step (see Sect. 2.3). Type II and III errors occur when light fluoresced by dye 1 is absorbed by dye 2 and re-emitted at a higher wavelength. These errors result in reduced measured intensity from system 1 and increased fluorescence intensity from system 2. Type II and III errors are negligible if the dye solutions are "optically thin" (i.e., concentrations are sufficiently low to produce negligible absorption over the path length of interest) (Melton and Lipp 2003).

Fluorescein sodium salt (CAS# 518-47-8) was paired with the argon-ion laser. Fluorescein possesses a high quantum yield, is water soluble, exhibits low sensitivity to temperature changes (Crimaldi 2008), and is non-toxic (Smart and Laidlaw 1977). Fluorescein's susceptibility to photobleaching is minimal for most PLIF applications (Larsen and Crimaldi 2006). Oxazine 725 (CAS# 24796-94-9) was paired with the krypton-ion laser. Because the properties of dyes vary with pH (Martin and Lindqvist 1975; Walker 1987) and solvent (Ware et al. 1983), the absorption and fluorescence spectra for fluorescein and oxazine 725 in tap water (pH $\approx$ 7) were measured using a spectrofluorometer (Fig. 2). The absorption coefficients, ε, were measured using a small tank of uniform dye concentration and were used to ensure the experiment in Sect. 3 was performed in an optically thin regime. The peak absorbance and fluorescence, as well as the absorption coefficient, are shown in Table 1. A bandpass with filter centered at 555 nm and with full width at half maximum of 30 nm (Omega Optical) was paired with fluorescein's emission spectra, and a longpass filter with a 50% cut-on edge at 660 nm (Omega Optical) was paired with oxazine 725.

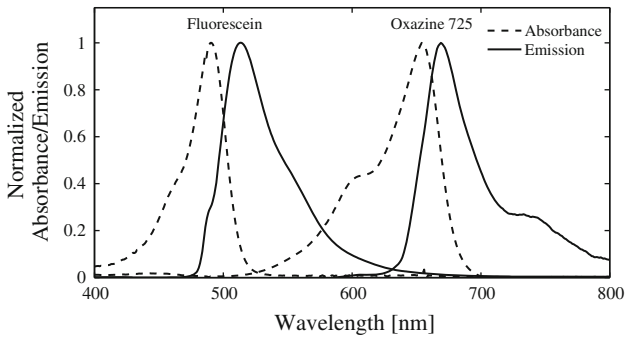

Fig. 2 Normalized absorption/emission spectra for fluorescein and oxazine 725

Table 1 Measured properties of fluorescein and oxazine 725 in aqueous solutions

Dye	Peak abs. (nm)	Peak em. (nm)	ε ($cm^{-1}\,M^{-1}$)
Fluorescein	491	514	1.40e5
Oxazine 725	656	668	2.33e5

2.3 Image processing

2.3.1 *Image rectification*

Because each camera views the image plane from a separate location and angle, the images are rectified to a common viewpoint normal to the image plane. A calibration grid is placed in the image plane, and calibration images are used to infer extrinsic parameters about the camera locations (Zhang 1999; Heikkila and Silven 1997). From these parameters, a standard 2D spatial transformation is applied to correct skew and translation errors (e.g., Brown 1992). The transformation rectifies the images to within 0.5 pixels.

2.3.2 *Error correction*

A detailed discussion of existing post-processing techniques for single-dye PLIF images is found in Crimaldi (2008). These correction algorithms are used to correct errors caused by fluorescence from background dye, fluorescence saturation, laser attenuation, spatial variation in the light sheet, lens vignette, and variations in gain and offset (Crimaldi and Koseff 2001). A robust image processing algorithm uses the camera dark response, D, and a background image of uniform dye concentration, B, to correct for these errors on a pixel-by-pixel basis in a Cartesian grid. For an optically thin system, concentrations are given by Crimaldi (2008):

$$C_n(i,j) = b_n \frac{I_n(i,j) - B_n(i,j)}{B_n(i,j) - D(i,j)} \quad (1)$$

where I_n is the intensity field for the nth image, and b_n is the background dye concentration for the nth image, interpolated from images before and after the experiment. As discussed in Sect. 2.2, the three additional types of errors introduced by Coppeta and Rogers (1998) are minimized by careful selection of dyes and optical filters, as well as by operating in an optically thin regime. Further correction of type I crosstalk can be performed.

If type I crosstalk occurs in a two-channel PLIF system, the pixel intensity in the two background images is:

$$B_{1,n} = \alpha_1 b_{1,n} + D_1 \tag{2}$$

and

$$B_{2,n} = \alpha_2 b_{2,n} + \alpha_1 \lambda b_{1,n} + D_2 \tag{3}$$

where λ is the crosstalk occurring from channel 1 to channel 2 and α_1 and α_2 are collections of concentration-independent constants. Similarly, the fluorescence intensity in the nth images can be expressed as:

$$I_{1,n} = \alpha_1 [C_{1,n} + b_{1,n}] + D_1 \tag{4}$$

and

$$I_{2,n} = \alpha_2 [C_{2,n} + b_{2,n}] + \alpha_1 \lambda [C_{1,n} + b_{1,n}] + D_1 \tag{5}$$

Equations 2–5 can be combined to give expressions for $C_{1,n}$ and $C_{2,n}$ that do not include any explicit references to α_1 or α_2:

$$C_{1,n}(i,j) = b_{1,n} \frac{I_{1,n} - B_{1,n}}{B_{1,n} - D_1} \tag{6}$$

and

$$C_{2,n}(i,j) = b_{2,n} \frac{I_{2,n} - B_{2,n} - \lambda [I_{1,n} - B_{1,n}]}{B_{2,n} - D_2 - \lambda [B_{1,n} - D_1]} \tag{7}$$

If no crosstalk occurs, λ is equal to zero, and the correction algorithm for channel 2 is identical to Eq. 1. The constant λ varies based on parameters of the system such as camera spectral sensitivity, relative laser power for both lasers, and the pH of the fluid. Therefore, λ is calculated empirically as discussed in Sects. 2.4 and 3.

2.4 System validation

System validation experiments were conducted in a well-mixed 16 L tank initially containing background concentrations of 4 ppb fluorescein and 1 ppb oxazine. The tank was dosed with five concentrations of fluorescein (in constant steps from 0 to 4 ppb above the background) and five concentrations of oxazine (in constant steps from 0 to 16 ppb above the background) in all 25 possible combinations. Each of the resulting concentration combinations was imaged with the two-channel PLIF system, and the fluorescence was averaged across each of the images. The resulting fluorescence data were post-processed with Eqs. 6 and 7. λ, b_1, and b_2 were determined via a three-parameter least-squares analysis that minimized collective errors on C_1 and C_2. Resulting normalized concentrations for representative cases are shown in Fig. 3.

To demonstrate linearity within and independence between the two PLIF channels, linear regressions were fit to both data channels for each sequence of dye additions. When fluorescein was sequentially added, the fluorescein channel showed a linear 1:1 response (blue line in Fig. 3a), but the oxazine channel showed no response (red line in Fig. 3a). Likewise, when oxazine was added, the oxazine channel showed a linear 1:1 response (red line in Fig. 3b), but the fluorescein channel showed no response (blue line in Fig. 3b). The regressions to same-dye response were within 0.005 of 1:1 slopes, with $r^2 > 0.999$, demonstrating channel linearity within 0.5% over the range of concentrations tested. The slopes of the off-dye regressions had magnitudes less than 0.003, demonstrating channel independence within 0.3%.

3 Two-jet experiment

The two-channel PLIF system was used to quantify two interacting scalar fields in a pair of parallel turbulent jets (Fig. 4). The jets issued from 3.9-mm nozzles, oriented horizontally, and separated by 2.5 cm. The upper jet was dosed with fluorescein ($\tilde{C}_1 = 0.05$ ppm) and the lower with oxazine ($\tilde{C}_2 = 0.08$ ppm). Each jet was driven with a pulseless gear pump at 145 ml/min, producing a bulk velocity of 20.2 cm/s ($Re = 790$, defined on the nozzle diameter). The jets issued into an ambient 1 cm/s flow that contained uniform background concentrations of both dyes for error correction purposes (see Eq. 1). The ambient flow was laminar and shear-free and prevented jet fluid from accumulating in the test section. The jets exited the nozzles in a laminar potential core, but became turbulent for $x \geq 5$ cm. The scalar fields were imaged in a 14 cm × 14 cm region located at $-7 \leq z \leq 7$ cm and $15 \leq x \leq 29$ cm.

A series of 2,000 images of instantaneous scalar structure was acquired at 0.33 Hz on each channel of the PLIF system and processed as discussed in Sect. 3 At 2,000 images, running averages of all statistics reported show convergence within 1%. The coefficient λ was determined from a separate experiment with a single fluorescein jet, while b_1 and b_2 were calibrated using images of known uniform concentrations of fluorescein and oxazine. Except as noted, fluorescein and oxazine concentrations C_1 and C_2 were then normalized by their respective source concentrations $\tilde{C}_1$ and $\tilde{C}_2$. The normalized concentrations at any

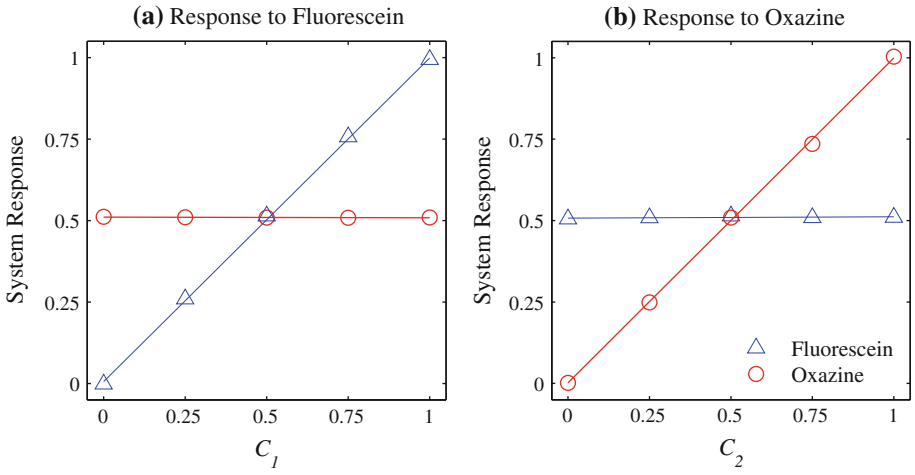

Fig. 3 Representative system response (Eqs. 6, 7) for two-channel PLIF validation experiments for changes in fluorescein concentration, C_1, and oxazine concentration, C_2. Two representative experiments are shown: **a** the addition of fluorescein at a constant oxazine concentration and **b** the addition of oxazine at a constant fluorescein concentration. The *lines* are least-squares fits to the data

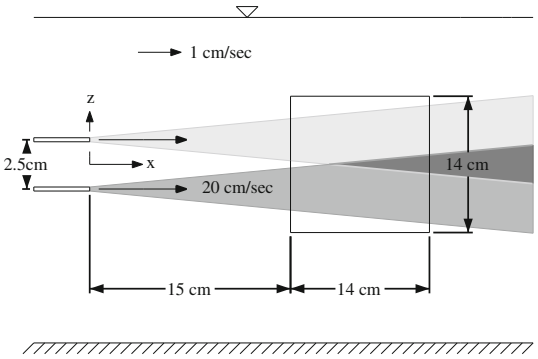

Fig. 4 Two-jet experiment setup. The upper and lower jets emitted fluorescein and oxazine, respectively

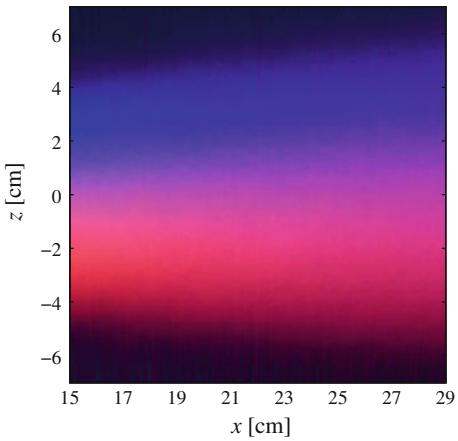

Fig. 5 Time-averaged composite image of the two normalized jet concentrations. For clarity, 10 $<C_1>$ and 10 $<C_2>$ are plotted, using the color scheme shown in Fig. 6. Flow is from *left* to *right*

location can be decomposed in terms of mean and fluctuating components $C = <C> + c'$.

The mean spreading and overlap of the two scalar fields is shown in a composite image comprised of the average concentrations from each PLIF channel (Fig. 5). A two-dimensional false-color scheme (Fig. 6) is used to simultaneously display normalized values of C_1 and C_2 in any combination. This color scheme displays values of pure C_1 and C_2 along the horizontal and vertical axes, with various combinations of C_1 and C_2 shown by the off-axis colors. Profiles of the normalized mean concentrations are skewed Gaussians (Fig. 7a), where the skew results from jet interactions. Turbulence from one jet mixes and elongates the interior tail of the concentration profile for the other jet. The same effect erodes the concentrations along the jet axes at $z = \pm 1.5$ cm (dashed lines), resulting in peak concentrations outside of each axis. Profiles of the normalized RMS concentration fluctuations exhibit a similar interior skew (Fig. 7b) in addition to a flattening (kurtosis) near the jet core typical of turbulent round jets (Wygnanski and Fiedler 1969; Webster et al. 2001).

The mean local mixing parameter, $<C_1C_2>$, can be decomposed as:

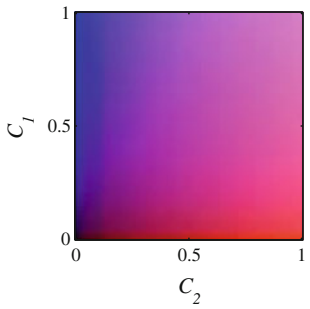

Fig. 6 False-color scheme for encoding mixed concentrations from the two-channel PLIF system. C_1 and C_2 are the concentrations of fluorescein and oxazine, respectively, normalized to the concentration at the jet exit

$$<C_1C_2> = <C_1><C_2> + <c_1'c_2'> \quad (8)$$

where the two terms on the RHS correspond to contributions from the mean and fluctuating concentration fields, respectively. The three components in Eq. 8 are shown

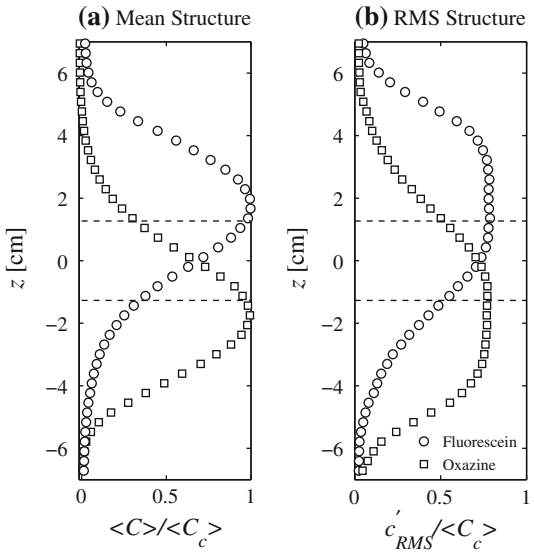

Fig. 7 Time-averaged vertical concentration profiles, normalized to the local mean centerline concentration, $<C_c>$ (*left*) and RMS profiles for the parallel jet experiment, normalized to the local centerline concentration (*right*). Profiles were averaged over $21 < x < 24$ cm. *Dashed lines* show the location of the jet axes

graphically in Fig. 8. By definition, $<C_1><C_2>$ is everywhere non-negative, with positive values corresponding to regions where the mean concentration fields overlap. The correlation $<c_1'c_2'>$ is negative over the central region of the domain ($|z| < 3$), with regions of positive fluctuation correlations near $z = \pm 4$ cm. An understanding of these average correlations requires an investigation of the instantaneous scalar fields.

A representative composite image of the instantaneous scalar fields C_1 (blue) and C_2 (red) is shown in Fig. 9, again using the false-color scheme from Fig. 6. Purple filaments correspond to regions where turbulent stirring and

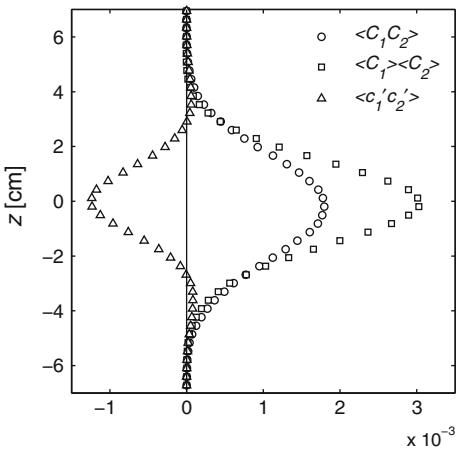

Fig. 8 Normalized mixing statistics for the two jet experiments, calculated from 2,000 instantaneous measurements and averaged over $21 < x < 24$ cm

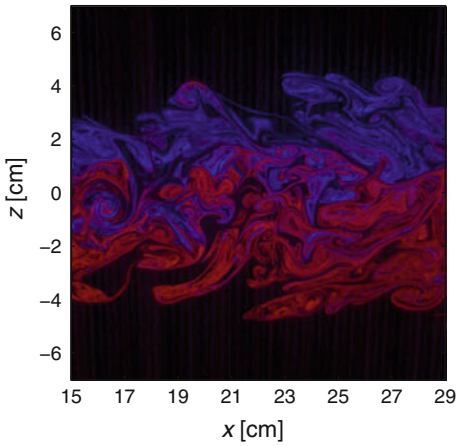

Fig. 9 Instantaneous composite image of an x–z slice through the two jet system. The two scalars are encoded in the false-color scheme shown in Fig. 6. Flow is from *left* to *right*

molecular diffusion have combined to produce an overlap between the blue and red scalar fields. The purple regions can be calculated and displayed explicitly as the scalar mixing product C_1C_2 (Fig. 10). Here, instantaneous values of C_1C_2 are quantified where white regions have no mixing and gray regions have some mixing between C_1 and C_2.

Contributions to the scalar mixing product C_1C_2 come from the mean scalar fields as well as the fluctuating scalar fields c_1' and c_2'. Contributions from the fluctuating scalar product $c_1'c_2'$, which can be of either sign, are shown in Fig. 11. Here, negative values of $c_1'c_2'$ are shown in blue, while positive values are shown in red. Regions with no fluctuating scalar product appear in white. The central region $-2 < z < 2$ cm is dominated by filaments where $c_1'c_2'$ is strongly negative (dark blue), corresponding to events where turbulent intrusions of fluid from one jet displace fluid from the second jet. If the jet containing C_1 does the displacing, then locally $c_1' > 0$ and $c_2' < 0$, and vice

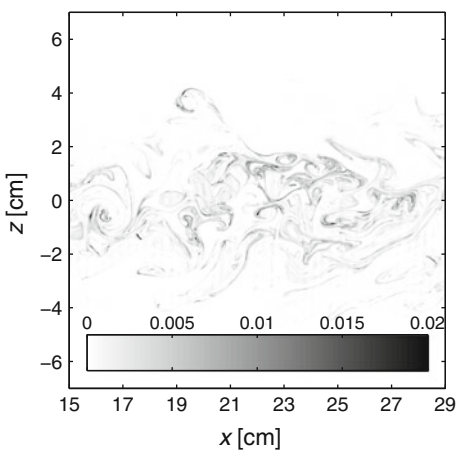

Fig. 10 Instantaneous field of the mixing product C_1C_2, corresponding to the composite image shown in Fig. 9

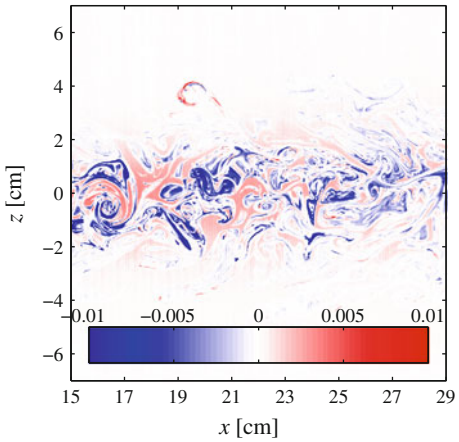

Fig. 11 Instantaneous field of $c_1'c_2'$

versa. Also visible in the central region are regions where $c_1'c_2'$ is weakly positive (light red). These are not mixing regions, but, instead, regions where C_1 and C_2 are both zero (corresponding to the black interior regions in Fig. 9), resulting in $c_1' < 0$ and $c_2' < 0$. These weakly positive regions are not strong enough to overcome the strongly negative ones, and the average fluctuating scalar product $< c_1'c_2' >$ in the central region is thus negative (see triangle symbols in Fig. 8). Outside the central region, in the vicinity of $z = \pm 4$ cm, $< c_1'c_2' >$ is positive. A representative positive contribution to this average is seen in the fluctuating scalar field $< c_1'c_2' >$ near $x = 20$ cm, $z = 4$ cm in Fig. 11. Such contributions presumably correspond to a scalar from one jet that quickly protrudes (at small x) deep into the region of the second jet, where the two scalars then evolve in x in a shared turbulent flow whose vortical structures impart correlations on the scalar field (Crimaldi et al. 2008).

It is important to note that the two-channel PLIF system described in the present study permits direct visualization and quantification of the instantaneous events that contribute to various mixing statistics involving two initially distant scalar fields. In previous studies, the mean statistics (Fig. 8) were inferred indirectly using the method of inference (Warhaft 1981, 1984; Tong and Warhaft 1995; Costa-Patry and Mydlarski 2008).

4 Conclusion

A novel two-channel PLIF technique is presented that is capable of measuring two scalars simultaneously and independently from each other. The technique is comprised of two independently operated PLIF systems. A validation experiment shows the system's ability to quantify concentration fields of both scalars including in regions where the two scalars overlap with errors less than 1%.

The system is used to investigate scalar interactions between two parallel jets. Instantaneous views of the two scalar fields, and their correlations are shown which help describe the physics behind multiple scalar mixing. The two-channel PLIF system is well-suited for studies of mixing phenomena involving multiple scalars and reaction problems in the high-Damköhler limit (i.e., problems where reaction is much slower than advection).

Acknowledgments This work was supported by the National Science Foundation under Award No. OCE-0849695.

References

Arcoumanis C, McGuirk J, Palma J (1990) On the use of fluorescent dyes for concentration measurements in water flows. Exp Fluids 10(2–3):177–180. doi:10.1007/BF00215028

Becker HA, Booth BD (1975) Mixing in the interaction zone of two free jets. Am Inst Chem Eng J 21(5):949–958. doi:10.1002/aic.690210517

Brown L (1992) A survey of image registration techniques. ACM Comput Surv 24(4):325–376. doi:10.1145/146370.146374

Bruchhausen M, Guillard F, Lemoine F (2005) Instantaneous measurement of two-dimensional temperature distributions by means of two-color planar laser induced fluorescence (PLIF). Exp Fluids 38(1):123–131. doi:10.1007/s00348-004-0911-2

Cetegen BM, Mohamad N (1993) Experiments on liquid mixing and reaction in a vortex. J Fluid Mech 249:391–414. doi:10.1017/S0022112093001223

Cetegen BM, Sirignano WA (1990) Study of mixing and reaction in the field of a vortex. Combust Sci Technol 72(4):157–181. doi:10.1080/00102209008951646

Champagne FH, Wygnanski IJ (1971) An experimental investigation of coaxial turbulent jets. Int J Heat Mass Transf 14(9):1445–1464. doi:10.1016/0017-9310(71)90191-8

Coppeta J, Rogers C (1998) Dual emission laser induced fluorescence for direct planar scalar behavior measurements. Exp Fluids 25(1):1–15. doi:10.1007/s003480050202

Costa-Patry E, Mydlarski L (2008) Mixing of two thermal fields emitted from line sources in turbulent channel flow. J Fluid Mech 609:349–375. doi:10.1017/S0022112008002425

Crimaldi JP (2008) Planar laser induced fluorescence in aqueous flows. Exp Fluids 44(6):851–863. doi:10.1007/s00348-008-0496-2

Crimaldi JP, Koseff JR (2001) High-resolution measurements of the spatial and temporal scalar structure of a turbulent plume. Exp Fluids 31(1):90–102. doi:10.1007/s003480000263

Crimaldi JP, Cadwell JR, Weiss JB (2008) Reaction enhancement of isolated scalars by vortex stirring. Phys Fluids 20(7). doi:10.1063/1.2963139

Duplat J, Villermaux E (2008) Mixing by random stirring in confined mixtures. J Fluid Mech 617:51. doi:10.1017/S0022112008003789

Fujisawa N, Nakamura K, Srinivas K (2004) Interaction of two parallel plane jets of different velocities. J Vis 7(2):135–142. doi:10.1007/BF03181586

Grandmaison E, Zettler N (1989) Turbulent mixing in coflowing plane jets. Can J Chem Eng 67(6):889–897. doi:10.1002/cjce.5450670604

Heikkila J, Silven O (1997) A four-step camera calibration procedure with implicit image correction. In: IEEE computer society

conference on computer vision and pattern recognition, pp 1106–1112. doi:10.1109/CVPR.1997.609468
Hodgson JE, Moawad AK, Rajaratnam N (1999) Concentration field of multiple circular turbulent jets. J Hydraul Eng Res 37(2):249–256. doi:10.1080/00221689909498309
Karasso PS, Mungal MG (1997) PLIF measurements in aqueous flows using the Nd: YAG laser. Exp Fluids 23(5):382–387. doi:10.1007/s003480050125
Kling K, Mewes D (2004) Two-colour laser induced fluorescence for the quantification of micro- and macromixing in stirred vessels. Chem Eng Sci 59(7):1523–1528. doi:10.1016/j.ces.2004.01.015
Koochesfahani MM, Dimotakis PE (1986) Mixing and chemical reactions in a turbulent liquid mixing layer. J Fluid Mech 170:83–112. doi:10.1017/S0022112086000812
Larsen LG, Crimaldi JP (2006) The effect of photobleaching on PLIF. Exp Fluids 41(5):803–812. doi:10.1007/s00348-006-0205-y
Lavertu TM, Mydlarski L, Gaskin SJ (2008) Differential diffusion of high-Schmidt-number passive scalars in a turbulent jet. J Fluid Mech 612:439–475. doi:10.1017/S0022112008003224
Lehwald A, Thevenin D, Zahringer K (2010) Quantifying macro-mixing and micro-mixing in a static mixer using two-tracer laser-induced fluorescence. Exp Fluids 48:823–836
Martin MM, Lindqvist L (1975) The pH dependence of fluorescein fluorescence. J Lumin 10(6):381–390. doi:10.1016/0022-2313(75)90003-4
Melton LA, Lipp CW (2003) Criteria for quantitative PLIF experiments using high-power lasers. Exp Fluids 35(4):310–316. doi:10.1007/s00348-003-0632-y
Pani B, Dash R (1983) Three-dimensional single and multiple free jets. J Hydraul Eng 109(2):254. doi:10.1061/(ASCE)0733-9429(1983)109:2(254)
Robinson GA, Lucht RP, Laurendeau NM (2008) Two-color planar laser-induced fluorescence thermometry in aqueous solutions. Appl Opt 47(15):2852–2858. doi:10.1364/AO.47.002852
Sakakibara J, Adrian RJ (1999) Whole field measurement of temperature in water using two-color laser induced fluorescence. Exp Fluids 26(1–2):7–15. doi:10.1007/s003480050260
Smart PL, Laidlaw IMS (1977) An evaluation of some fluorescent dyes for water tracing. Water Resour Res 13(1):15–33
Stapountzis H, Westerweel J, Bessem JM, Westendorp A, Nieuwstadt FTM (1992) Measurement of product concentration of two parallel reactive jets using digital image processing. Appl Sci Res 49(3):245–259. doi:10.1007/BF00384625
Su LK, Clemens NT (1999) Planar measurements of the full three-dimensional scalar dissipation rate in gas-phase turbulent flows. Exp Fluids 27(6):507–521. doi:10.1007/s003480050375
Tong C, Warhaft Z (1995) Passive scalar dispersion and mixing in a turbulent jet. J Fluid Mech 292:1–38. doi:10.1017/S0022112095001418
Walker DA (1987) A fluorescence technique for measurement of concentration in mixing liquids. J Phys E Sci Instrum 20(2):217–224. doi:10.1088/0022-3735/20/2/019
Wang CS, Lin YF, Sheu MJ (1993) Measurements of turbulent inclined plane dual jets. Exp Fluids 16(1):27–35. doi:10.1007/BF00188502
Wang HJ, Davidson MJ (2003) Jet interaction in a still ambient fluid. J Hydraul Eng 129(5):349–357. doi:10.1061/(ASCE)0733-9429(2003)129:5(349)
Ware B, Cyr D, Gorti S, Lanni F (1983) Electrophoretic and frictional properties of particles in complex media measured by laser light scattering and fluorescence photobleaching recovery. In: Dahneke BE (eds) Measurement of suspended particles by quasi-elastic light scattering.. Wiley, New York, pp 255–289
Warhaft Z (1981) The use of dual heat injection to infer scalar covariance decay in grid turbulence. J Fluid Mech 104:93–109. doi:10.1017/S0022112081002838
Warhaft Z (1984) The interference of thermal fields from line sources in grid turbulence. J Fluid Mech 144:363–387. doi:10.1017/S0022112084001646
Webster DR, Roberts PJW, Ra'ad L (2001) Simultaneous DPTV/PLIF measurements of a turbulent jet. Exp Fluids 30(1):65–72. doi:10.1007/s003480000137
Wygnanski I, Fiedler H (1969) Some measurements in the self-preserving jet. J Fluid Mech 38(03):577–612. doi:10.1017/S0022112069000358
Yuu S, Shimoda F, Jotaki T (1979) Hot wire measurement in the interacting two-plane parallel jets. AIChE J 25(4):676–685. doi:10.1002/aic.690250414
Zhang Z (1999) Flexible camera calibration by viewing a plane from unknown orientations. In: International Conference on Computer Vision, Corfu, Greece, pp 666–673